Dispersive ionospheric Alfvén resonator

• D Pokhotelov, Oleg A Pokhotelov, D. Pokhotelov, A. Streltsov, V. Khruschev, Michel Parrot

JOURNAL OF GEOPHYSICAL RESEARCH, VOL. 105, NO. A4, PAGES 7737–7746, APRIL 1, 2000

Dispersive ionospheric Alfvén resonator

Oleg A. Pokhotelov,[1] D. Pokhotelov,[2] A. Streltsov,[2]
V. Khruschev,[1] and M. Parrot[3]

Abstract. A new model of the ionospheric Alfvén resonator (IAR) including the effect of wave frequency dispersion is presented. It is shown that the shear Alfvén waves in the IAR are coupled to the compressional mode through the boundary conditions at the ionosphere. This coupling results in the appearance of the Hall dispersion and subsequent shift of the IAR frequency spectrum. The excitation mechanism involving the IAR interaction with the magnetospheric convective flow is considered. It is shown that the Hall dispersion of the IAR eigenmode increases the growth rate of the feedback instability. However, for the observed values of ionospheric conductivity this effect is not very high. It is shown that the physical mechanism of the feedback instability is similar to the Čerenkov radiation in collisionless plasmas. The IAR eigenfrequencies and growth rates are evaluated for the case of exponential variation of the Alfvén velocity with altitude in the topside ionosphere.

1. Introduction

The concept of the ionospheric Alfvén resonator (IAR) has been the subject of a great deal of research during recent years. The IAR arises due to the strong increase in the Alfvén velocity with altitude, which results in wave reflection from velocity gradients and formation of a resonance cavity in the topside ionosphere. The idea of IAR was originally suggested by *Polyakov* [1976] and has been extensively studied by a number of authors [e.g., *Polyakov and Rapoport*, 1981; *Belyaev et al.*, 1987, 1990; *Lysak*, 1991; *Trakhtengertz and Feldstein*, 1991]. The most peculiar features of IAR are observed in the auroral zone, where the structure of currents and electric fields is controlled by interaction and propagation of ULF waves in the topside ionosphere. Recently, experimental evidence for the existence of IAR at high latitudes was confirmed by *Belyaev et al.* [1999] by using highly sensitive, two-component induction magnetometer measurements from Kilpisjärvi Observatory (Finland).

The principal mechanism of IAR destabilization is connected with the sudden enhancement of magnetospheric convection during magnetic storms, which results in an instability, called the "fast feedback instability" [*Lysak*, 1991] in order to distinguish it from the slow feedback instability of the global ionosphere-magnetosphere resonator studied by *Atkinson* [1970], *Sato and Holzer* [1973], and *Sato* [1978]. As the instability develops, part of the energy of the convective flow is transferred to the IAR eigenmodes. The theory of fast feedback instability was substantially developed by *Lysak* [1991] and *Trakhtengertz and Feldstein* [1991].

In this paper we will generalize the previous analysis by incorporating the dispersion of shear Alfvén waves in the ionosphere-magnetosphere coupled system. We will show that this dispersion is produced by the ionospheric Hall current which arises due to the coupling of shear Alfvén and fast magnetosonic (compressional) waves in the ionosphere. The deceleration of the Alfvén phase velocity due to the Hall dispersion may increase the rate of energy transfer from the convective flow to IAR eigenmodes and overcome the dissipation rate due to the leakage of energy through the IAR upper boundary. The physical mechanism of such an instability, which we will term below as "feedback instability", is similar to the usual Čerenkov radiation in collisionless plasma.

The paper is organized as follows: Section 2 describes the boundary conditions of the resonant cavity at the ionospheric and magnetospheric ends. The analysis of the dispersive ionospheric Alfvén resonator is given in section 3. The dispersion relation for the feedback instability is presented in section 4. Excitation of dispersive eigenoscillations by the feedback instability in the low-conductivity ionosphere is considered in section 5. The case for a highly conductive ionosphere is analyzed in section 6. Our discussions and conclusions are found in section 7.

[1]Institute of Physics of the Earth, Moscow.
[2]Thayer School of Engineering, Dartmouth College, Hanover, New Hampshire.
[3]Laboratoire de Physique et Chimie de l'Environnement, Centre National de le Recherche Scientifique, Orléans, France.

Paper number 1999JA900480.
0148-0227/00/1999JA900480$09.00

2. Boundary Conditions in Dispersive IAR

It is known that the plasma density in the ionosphere and low-altitude magnetosphere varies strongly along the geomagnetic field lines. The typical scale for this variation is of the order of 10^3 km. This parallel plasma inhomogeneity leads to a strong variation in the background Alfvén speed, which in turn results in the appearance of a so-called ionospheric Alfvén resonance cavity. This cavity modifies the propagation of low frequency ULF waves near the ionosphere. Since the ionospheric cavity is localized at low altitudes (below $1-2\ R_E$), a straight magnetic field line approximation is used. The reference frame used in this study assumes that the external magnetic field $\mathbf{B}$ is directed along the z axis. For simplicity, the plasma is considered to be homogeneous across magnetic field lines.

The shear Alfvén and compressional modes in our model are described by the parallel component of the vector potential A and two scalar potentials Φ and Ψ. In this notation the total vector potential can be written as $\mathbf{A} = A\hat{\mathbf{z}} + \nabla_\perp \times (\Psi\hat{\mathbf{z}})$, where the second term represents the perpendicular component of the vector potential.

If all perturbed quantities vary as $\exp(-i\omega t)$, then the electric and magnetic field perturbations can be written in the following form:

$$\delta\mathbf{E}_\perp = -\nabla_\perp\Phi + i\omega\nabla_\perp \times \Psi\hat{\mathbf{z}}, \tag{1}$$

$$\delta\mathbf{B}_\perp = \nabla_\perp A \times \hat{\mathbf{z}} + \nabla_\perp\partial_z\Psi, \tag{2}$$

and

$$\delta\mathbf{B}_z = -\nabla_\perp^2\Psi, \tag{3}$$

where $\partial_z \equiv \partial/\partial z$, ω is the wave frequency, and $\hat{\mathbf{z}}$ is the unit vector along the external magnetic field. The parallel component of the vector potential A is related to the scalar potential Φ by

$$\partial_t A = -\partial_z\Phi. \tag{4}$$

Equation (4) represents the fact that the field-aligned electric field in our plasma is zero, that is, $E_z = -\partial_z\Phi + i\omega A = 0$. This is valid if the wavelengths of the considered waves are much larger then the collisionless electron skin depth.

The field-aligned current can be obtained by taking the parallel component of Ampère's law, $\nabla \times \delta\mathbf{B} = \mu_0\mathbf{j}$, given by

$$j_z = -\frac{1}{i\omega}\mu_0^{-1}\nabla_\perp^2\partial_z\Phi. \tag{5}$$

To describe the plasma motion, we start with the linearized ideal MHD equation

$$-i\omega\rho\mathbf{v} = \mathbf{j} \times \mathbf{B}, \tag{6}$$

where ρ is the plasma mass density, $\mathbf{j}$ is the plasma current density, and $\mathbf{v}$ is the fluid velocity. In ideal MHD the magnetic field is frozen into the plasma, and the hydrodynamic velocity $\mathbf{v}$ is defined by the relation $\mathbf{v} = (\delta\mathbf{E}_\perp \times \hat{\mathbf{z}})/B$. In equation (6) we neglected the thermal pressure gradient. The latter condition assumes the low-pressure approximation. Eliminating from (6) the plasma current density with the help of Ampère's law and Faraday's laws and rearranging, we obtain

$$(\omega^2/c_A^2)\delta\mathbf{E}_\perp - \nabla_\perp(\nabla_\perp \cdot \delta\mathbf{E}_\perp) + \nabla^2\delta\mathbf{E}_\perp = 0, \tag{7}$$

where $c_A = B/(\mu_0\rho)^{1/2}$ is the Alfvén velocity and μ_0 is the permeability of free space.

With the help of Faraday's law and (1), equation (7) can be written in the form of two scalar equations

$$\partial_z^2\Phi + (\omega^2/c_A^2)\Phi = 0, \tag{8}$$

and

$$\nabla^2\Psi + (\omega^2/c_A^2)\Psi = 0, \tag{9}$$

which describe the shear Alfvén and compressional modes in the ionospheric plasma.

These equations should be supplemented by the proper boundary conditions for the ionosphere ($z = 0$) and at infinity ($z \to \infty$). The boundary conditions for the ionosphere are obtained from Ampère's law. Applying $(\nabla\cdot)$ and $(\nabla\times)_z$ to this equation, we obtain

$$\nabla \cdot \mathbf{j} = 0, \tag{10}$$

and

$$\nabla^2\delta B_z = -\mu_0(\nabla \times \mathbf{j})_z. \tag{11}$$

Equation (10) represents the electric current continuity equation, while (11) gives the supplementary relation which provides the connection between the potentials Ψ and Φ.

Following *Lysak* [1991] we consider the ionosphere as a conductive slab extending from $z = 0$ to $z = -\Delta z$. The neutral atmosphere ($-d < z < -\Delta z$) is considered as a vacuum region, and the solid Earth ($z < -d$) as a perfect conductor. Since the resistance between the ionosphere and ground is much higher than that of ionosphere, we may neglect the field-aligned current flowing from the ionosphere to the atmosphere, and at $z = -\Delta z$ (the boundary between the ionosphere and atmosphere) we set $j_z(z = -\Delta z) = 0$. Taking into account this condition, integration of (10) gives

$$j_z(z = 0) = -\nabla_\perp \cdot \mathbf{J}_\perp, \tag{12}$$

where $\mathbf{J}_\perp$ is the perpendicular ionospheric current integrated from $z = -\Delta z$ to $z = 0$. Positive j_z corresponds to the current flowing out of the ionosphere. Note also that the perpendicular electric field, and thus the scalar potentials, must be continuous across the boundary at $z = 0$.

In the thin slab approximation the conductive layer may be characterized by the height-integrated Pedersen and Hall conductivities Σ_P and Σ_H, respectively. Thus Ohm's law integrated across the ionosphere with $\mathbf{E}_\perp$ replaced by (1) can be written as

$$\mathbf{J}_\perp = -\Sigma_P \nabla_\perp \Phi + \Sigma_H \nabla_\perp \times \Phi \hat{\mathbf{z}}$$
$$+ i\omega\Sigma_H \nabla_\perp \Psi + i\omega\Sigma_P \nabla_\perp \times \Psi \hat{\mathbf{z}}, \quad (13)$$

For simplicity, the Hall and Pedersen conductivities are assumed to be uniform. Substituting (13) into (12) and using (5), we write the current continuity equation as

$$c_{A0}\partial_z \Phi + i\omega\alpha_P \Phi + \omega^2 \alpha_H \Psi = 0, \quad (14)$$

where $\alpha_P = \Sigma_P / \Sigma_w$ and $\alpha_H = \Sigma_H / \Sigma_w$ are the ratios of the height-integrated Pedersen and Hall conductivities to the wave conductivity $\Sigma_w = 1/\mu_0 c_{A0}$, and all the values are taken at $z = 0$.

Integration of equation (11) with the help of (3) and (13) gives

$$\partial_z \Psi + \Delta z \nabla_\perp^2 \Psi + c_{A0}^{-1}(\alpha_H \Phi + i\omega\alpha_P \Psi) = \partial_z \Psi(-\Delta z). \quad (15)$$

The right-hand side of (15) is defined at $z = -\Delta z$. In the neutral atmosphere ($-d < z < -\Delta z$), under the condition that Ψ vanishes on the surface ($z = -d$) of the perfectly conducting Earth, it is given by $\Psi = C\sinh[-k_\perp(z+d)]/\sinh(-k_\perp d)$ with C an arbitrary constant [*Yoshikawa and Itonaga*, 1996]. If the wavelength is much smaller than the atmospheric depth ($k_\perp d \gg 1$), Ψ scales as $\exp(k_\perp z)$, that is, falls off exponentially toward the ground. Using this condition, we set $\partial_z \Psi(-\Delta z) = k_\perp \Psi$, where $k_\perp$ is the perpendicular wave number. Replacing $\nabla_\perp^2$ with $-k_\perp^2$ in (15) and using the thin slab approximation, $\Delta z \to 0$, we obtain

$$\partial_z \Psi - k_\perp \Psi + c_{A0}^{-1}(\alpha_H \Phi + i\omega\alpha_P \Psi) = 0. \quad (16)$$

Finally, we have to specify the boundary conditions at the magnetospheric end, that is, at $z \to \infty$. To simplify the problem, we follow the method suggested by *Trakhtengertz and Feldstein* [1991] and assume that at $z \to \infty$ only outgoing solution exists. This corresponds to the so-called radiation condition at the magnetospheric end of IAR. Equations (8) and (9) with boundary conditions (14) and (16) at the ionosphere and the radiation conditions for shear Alfvén and compressional modes at infinity form a closed set of equations necessary for the study of IAR eigenmodes.

3. Dispersive Ionospheric Alfvén Resonator

Following *Lysak* [1991] and *Trakhtengertz and Feldstein* [1991] we choose the Alfvén velocity profile in the resonator as

$$c_A^2(z) = \frac{c_{A0}^2}{\varepsilon^2 + \exp(-2z/L)}, \quad (17)$$

where $\varepsilon \ll 1$. Physically, ε defines the ratio of the Alfvén velocity c_{AI} in the ionosphere to that in the outer magnetosphere c_{AM}. According to (17) they are related to this parameter as $c_{AI}/c_{MI} = \varepsilon/(1+\varepsilon^2)^{1/2} \simeq \varepsilon$. Thus $c_{AI} \simeq c_{A0}$ and $c_{AM} \simeq c_{A0}/\varepsilon$.

By substituting $x = x_0 e^{-z/L}$ and $x_0 = \omega L/c_{A0}$, (8) is transformed into the Bessel equation [e.g., *Lysak*, 1991]

$$\partial_x^2 \Phi + x^{-1}\partial_x \Phi + (1 + \varepsilon^2 x_0^2/x^2)\Phi = 0. \quad (18)$$

The solution of this equation, which satisfies the radiation condition at infinity, is

$$\Phi(x) = \Phi_0 J_{-ix_0\varepsilon}(x), \quad (19)$$

where Φ_0 is a constant, $x_0\varepsilon \ll 1$, and $J_\nu(x)$ is a Bessel function of complex index and complex argument.

Similarly, the solution to equation (9) in the limit $x_0\varepsilon \ll 1$ is given by

$$\Psi(x) = \Psi_0 J_{k_\perp L}(x), \quad (20)$$

where Ψ_0 is constant and we choose the solution which decreases with the altitude.

According to Meissnel's formula [e.g., *Watson*, 1948], in the region of the ionospheric sheet ($x \simeq x_0$) the Bessel function scales as $J_{k_\perp L}(x) \propto \exp(-k_\perp z)$ in the $k_\perp L \gg 1$ limit and $\partial_z \Psi = -k_\perp \Psi$. Therefore the first term in (16), involving the derivative of Ψ with respect to z, is equal to the second term in our approximation. Thus the compressional mode falls off as $\exp(-k_\perp |z|)$ on both sides of the ionospheric sheet.

Thus boundary condition (16) reduces to

$$\Psi = \frac{c_{A0}^{-1} L \alpha_H}{2k_\perp L - ix_0\alpha_p}\Phi, \quad (21)$$

where all the values are taken at $x = x_0$.

From (19)-(21) it follows that

$$\Psi = \frac{c_{A0}^{-1} L \alpha_H \Phi_0 J_{-ix_0\varepsilon}(x_0)}{(2k_\perp L - ix_0\alpha_p) J_{k_\perp L}(x_0)} J_{k_\perp L}(x), \quad (22)$$

Substituting (21) into condition (14), we finally obtain

$$\partial_x \Phi + (i\alpha_P + \frac{x_0 \alpha_H^2}{2k_\perp L - ix_0\alpha_P})\Phi = 0. \quad (23)$$

Expression (23) without the Hall dispersion term coincides with that obtained by *Lysak* [1991] and *Trakhtengertz and Feldstein* [1991]. This additional term describes the coupling between the shear and compressional Alfvén modes. According to (10) and (11) the inclusion of the Hall dispersion in the boundary condition (23) is necessary in order to satisfy Ampère's law.

Substituting the solution (19) into boundary condition (23), we obtain the dispersion relation for IAR eigenfrequencies

$$\frac{J'_{-ix_0\varepsilon}(x_0)}{J_{-ix_0\varepsilon}(x_0)} = i\alpha_P + \frac{x_0\alpha_H^2}{2k_\perp L - ix_0\alpha_P}, \qquad (24)$$

where the prime denotes the derivative over the argument of the Bessel function.

In the low-conductivity case ($\alpha_P \ll 1$ and $\alpha_H \ll 1$), decomposing the dimensionless frequency x_0 into its real and imaginary parts, $x_0 = \eta + i\delta$, and assuming that the three quantities $x_0\varepsilon$, α_P, and $\alpha_H^2/k_\perp L$ are small, we obtain

$$\eta = \eta_{1m}\left(1 - \frac{\alpha_H^2}{2k_\perp L}\right), \qquad (25)$$

and

$$\delta = -\alpha_P - \frac{\varepsilon}{J_0^2(\eta_{1m})}, \qquad (26)$$

where η_{1m}, $m = 1, 2, 3,...$ are the zeroes of the J_1 function; for example, the first two roots of η_{1m} are 3.8 and 7.0 [cf. *Gradshteyn and Ryzhik*, 1980]. Similarly, for $J_0^2(\eta_{1m})$ we have 0.2 and 0.1.

It is seen from (25) that the inclusion in the model of the compressional mode leads to the small reduction in the resonant eigenfrequencies (red frequency shift) and provides dispersion for the shear Alfvén waves. Expression (26) describes the wave damping rate due to the Pedersen currents in a conductive layer (first term on the right-hand side of (26)) and wave energy leakage through the upper IAR wall (the second term). Terms describing the mode attenuation due to the Hall currents are neglected here because they are small quantities of the higher order $\sim 1/(k_\perp L)^2$. Inspecting values of $J_0^2(\eta_{1m})$, one may find that this attenuation is stronger for the higher harmonics.

The schematic plot of the perpendicular electric field $\delta\mathbf{E}_\perp$ of the fundamental IAR eigenmode for a weakly conductive ionosphere is shown in Figure 1 (solid curve). We recall that $\delta\mathbf{E}_\perp$ is defined by the relation (1), where the first term on the right-hand side gives the main contribution while the second one is considered as a small correction, that is, $\delta\mathbf{E}_\perp \simeq -i\mathbf{k}_\perp\Phi$ with Φ defined by (19). Owing to the low ionospheric conductivity it has antinodes both at the conductive layer and at the upper boundary of the IAR.

From (3) and (22) the compressional component of the magnetic field for the case of low conductivity takes the value

$$\delta B_\parallel(z \to 0) \simeq \frac{\alpha_H k_\perp J_0(\eta_{1m})}{2c_{A0}}\Phi_0. \qquad (27)$$

As the altitude increases, it rapidly ($\propto \exp(-k_\perp z)$) decays toward the magnetospheric end.

In the highly conductive ionosphere the IAR eigenfrequencies are close to the roots of the zero order Bessel function, $J_0(\eta_{0m}) = 0$ [e.g., *Trakhtengertz and Feldstein*, 1991]. The first two roots for η_{0m} are 2.4 and 5.5 [cf. *Gradshteyn and Ryzhik*, 1980]. From (27) it follows that the compression of the magnetic field in the highly conductive ionosphere vanishes and the Hall dispersion is not important. When the ionospheric conductivity is high the perpendicular component of the electric field of the fundamental eigenmode has nodes at both the lower and upper IAR boundaries. It is plotted schematically with a long-dashed curve in Figure 1.

4. Dispersion Relation for Feedback Instability

In this section we consider the generation of shear Alfvén waves in the presence of magnetospheric convection flow. We assume that the electric field $\mathbf{E}_0$, connected with this convection, penetrates the conductive ionospheric sheet and serves as the source of free energy necessary for the excitation of IAR eigenoscillations. For simplicity, we assume that the ionospheric conductivity is directly proportional to the density. This is a reasonable assumption as long as the ionospheric temperature and the neutral density do not vary significantly due to the field-aligned currents or subsequent

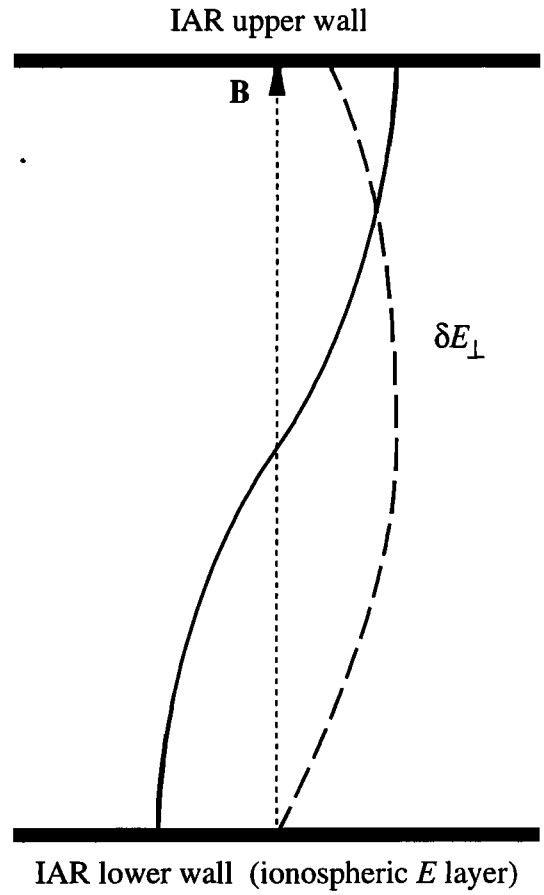

Figure 1. Perpendicular electric field $\delta E_\perp$ of the fundamental eigenmode when the ionspheric conductivity is low (solid curve) and when it is high (long-dashed curve).

particle precipitation [cf. *Lysak*, 1991]. Thus the variation of the height-integrated Pedersen and Hall conductivities can be written as

$$\delta\Sigma_P/\Sigma_P = \delta\Sigma_H/\Sigma_H = \delta n/n_0, \tag{28}$$

where δn is the perturbation of the ionospheric number density and n_0 is the equilibrium density due to the solar radiation. The ionospheric density satisfies a continuity equation which includes a source due to precipitation and losses due to recombination,

$$\partial_t n + \nabla_\perp \cdot (n\mathbf{v}_E) = S - R(n^2 - n_0^2), \tag{29}$$

where $\mathbf{v}_E = B^{-1}(\mathbf{E} \times \hat{\mathbf{z}})$, $\mathbf{E} = \delta\mathbf{E}_\perp + \mathbf{E}_0$ is the total electric field, S is the source term due to precipitation, and R is the recombination coefficient, which is of the order of 2×10^{-7} cm^3 s^{-1} [e.g., *Brown*, 1966]. Note that the recombination scales as the square of the density since an electron and ion must meet to recombine. In this model the source term is due to the precipitation and is proportional to the field-aligned current density $S = Qj_z$ [cf. *Atkinson*, 1970; *Sato and Holzer*, 1973; *Sato*, 1978] (here a positive current corresponds to precipitating electrons). The source term S depends, to lowest order, on the energy flux of the precipitating electrons [*Rees*, 1963].

In the steady state, the density is given by $n = (n_0^2 + S/R)^{1/2}$, where for strong precipitation, the second term dominates. The density perturbation can be found from the linearized equation (29). In the reference frame moving with the drift velocity $\mathbf{v}_0 = B^{-1}(\mathbf{E}_0 \times \hat{\mathbf{z}})$ it is given by

$$\frac{\delta n}{n_0} = -\frac{k_\perp^2 B^{-1}(\alpha_I^{-1} c_{A0}^{-1} L \partial_{x_0}\Phi - \Psi)}{x_0 + i\nu}, \tag{30}$$

where $\partial_{x_0}\Phi = \partial_x\Phi\,|_{x=x_0}$, $\nu = 2LRn_0/c_{A0} \ll 1$ is the dimensionless recombination frequency, $\alpha_I = (\Delta z/\lambda_{pi})\gamma_Q^{-1}$, $\lambda_{pi} = c/\omega_{pi}$ is the collisionless ion skin length, $\omega_{pi} = (n_0 e^2/\varepsilon_0 m_i)^{1/2}$ is the ion plasma frequency, m_i is the ion mass, e is the magnitude of the electronic charge, and $\gamma_Q = e\Delta z Q$ represents the number of additional electron-ion pairs created per incident electron. Normally, γ_Q is a nearly linear function of the incoming electron energy. It is about 100 for 10 keV electrons [*Rothwell et al.*, 1984]. According to *Lysak* [1991], $\Delta z \simeq \lambda_{pi} \simeq 10 - 30$ km. Therefore for the real ionospheric conditions, α_I is a small parameter of the order of $10^{-1} - 10^{-2}$.

In order to find the field-aligned current in the presence of the convection electric field, we use equation (12), in which $\mathbf{J}_\perp$ should be eliminated with the help of Ohm's law and $\mathbf{E} = \delta\mathbf{E}_\perp + \mathbf{E}_0$ with $\delta\mathbf{E}_\perp$ given by (1) and $\mathbf{E}_0$ being the large-scale electric field. After simple rearrangements with the help of (30) we obtain

$$j_z = ik_\perp^2 \Sigma_w \cdot [i\alpha_P\Phi + \frac{\sigma_\varphi \partial_{x_0}\Phi}{x_0 + i\nu} + \alpha_H c_{A0} x_0 L^{-1}(1 - \frac{\alpha_I \alpha_H^{-1}\sigma_\varphi}{x_0 + i\nu})\Psi], \tag{31}$$

where

$$\sigma_\varphi = -\frac{L}{\alpha_I c_{A0}}[\alpha_P(\mathbf{k}_\perp \times \mathbf{v}_0)_z + \alpha_H(\mathbf{k}_\perp \cdot \mathbf{v}_0)]. \tag{32}$$

Substituting the explicit expression for j_z from the parallel component of Ampère's law into equation (31) in the moving system of reference, we obtain the following boundary condition:

$$(1 - \frac{\sigma_\varphi}{x_0 + i\nu})\partial_{x_0}\Phi - i\alpha_P\Phi - \alpha_H c_{A0} x_0 L^{-1}(1 - \frac{\alpha_I\alpha_H^{-1}\sigma_\varphi}{x_0 + i\nu})\Psi = 0. \tag{33}$$

The connection between the Φ and Ψ potentials, which follows from equation (11), can be obtained similar to section 2 and now reads

$$\Psi = \frac{c_{A0}^{-1} L[\alpha_H\Phi - i\delta_\varphi(x_0 + i\nu)^{-1}\partial_{x_0}\Phi]}{2k_\perp L - ix_0\alpha_P[1 + \alpha_I\alpha_P^{-1}\delta_\varphi(x_0 + i\nu)^{-1}]}, \tag{34}$$

where

$$\delta_\varphi = -\frac{L}{c_{A0}\alpha_I}[\alpha_H(\mathbf{k}_\perp \times \mathbf{v}_0)_z - \alpha_P(\mathbf{k}_\perp \cdot \mathbf{v}_0)]. \tag{35}$$

By introducing φ as the angle between the wave vector and the direction of the drift velocity, expressions (32) and (35) can be rewritten as

$$\sigma_\varphi = -\frac{k_\perp L v_0 \alpha_C}{\alpha_I c_{A0}}\cos[\varphi - \arctan(\alpha_P/\alpha_H)], \tag{36}$$

and

$$\delta_\varphi = -\frac{k_\perp L v_0 \alpha_C}{c_{A0}\alpha_I}\sin[\varphi - \arctan(\alpha_P/\alpha_H)], \tag{37}$$

where $\alpha_C = (\alpha_P^2 + \alpha_H^2)^{1/2}$.

With the help of (19), (33), and (34), the dispersion equation for the feedback instability becomes

$$\{1 - \frac{\sigma_\varphi}{x_0 + i\nu} + i\frac{x_0\alpha_H\delta_\varphi(x_0 + i\nu)^{-1}[1 - \alpha_I\alpha_H^{-1}\sigma_\varphi(x_0 + i\nu)^{-1}]}{2k_\perp L - ix_0\alpha_P[1 + \alpha_I\alpha_P^{-1}\delta_\varphi(x_0 + i\nu)^{-1}]}\} \cdot \frac{J'_{-ix_{0\varepsilon}}(x_0)}{J_{-ix_{0\varepsilon}}(x_0)} = i\alpha_P + \frac{x_0\alpha_H^2(1 - \alpha_I\alpha_H^{-1}\sigma_\varphi(x_0 + i\nu)^{-1})}{2k_\perp L - ix_0\alpha_P[1 + \alpha_I\alpha_P^{-1}\delta_\varphi(x_0 + i\nu)^{-1}]}. \tag{38}$$

The dispersion equation (38) is rather complicated and can be solved in the general case only by numerical methods. However, we can simplify the problem and consider some limiting cases when the solution to this equation can be found analytically.

5. Feedback Instability in the Weakly Conductive Ionosphere

The dispersion relation (38) can be analyzed in two limiting cases of high and low ionospheric conductivities. In low-conductivity limit the solution to equation (38) is localized in the vicinity of the roots of the equation $J_1(\eta_{1m}) = 0$. According to *Lysak* [1991] the maximum of the feedback instability growth rate in the absence of the Hall dispersion is found in the vicinity of $\sigma_\varphi \simeq \eta_{1m}$ where δ_φ is negligible. Since the Hall dispersion in our problem is considered as a small correction, one should expect that in equation (38) the terms containing δ_φ may be neglected. The rigorous treatment (which leads to rather lengthy calculations) shows that accounting for these terms results in only a negligible shift in the expression for the critical velocity. Neglecting the small terms in equation (38), we get

$$(1-\frac{\sigma_\varphi}{x_0+i\nu})\frac{J'_{-ix_{0\varepsilon}}(x_0)}{J_{-ix_{0\varepsilon}}(x_0)} = i\alpha_P + \frac{x_0\alpha_H^2}{2k_\perp L}(1-\frac{\alpha_I\alpha_H^{-1}\sigma_\varphi}{x_0+i\nu}). \tag{39}$$

Expanding the Bessel functions in equation (39) in the vicinity of $x_0 \simeq \eta_{1m}$, we obtain

$$(x_0-\eta_{1m})(x_0-\sigma_\varphi+i\nu) = -\frac{x_0(x_0-\alpha_I\alpha_H^{-1}\sigma_\varphi+i\nu)\alpha_H^2}{2k_\perp L} - i(\alpha_P+\frac{\varepsilon}{J_0^2})(x_0+i\nu) + i\sigma_\varphi\frac{\varepsilon}{J_0^2}. \tag{40}$$

It follows from (40) that the appearance of the dimensionless frequency σ_φ is equivalent to the adding of a convective mode $x_0 = \sigma_\varphi$ (pumping wave) in the system. The modes become close to each other when $\sigma_\varphi \simeq \eta_{1m}$. The schematic plot of the dimensionless frequency η_0 as a function of dimensionless perpendicular wave number $k_\perp L$ is shown in Figure 2. It is seen that modes are separated due to the dispersion. For simplicity, we neglect the corrections due to recombination and leakage out of the upper boundary of the resonator and consider $\nu = \varepsilon = 0$. Note that both of these effects should just provide damping. Then we get

$$\left(1+\frac{\alpha_H^2}{2k_\perp L}\right)x_0^2 - x_0(\sigma_\varphi+\eta_{1m}-i\alpha_P+\sigma_\varphi\frac{\alpha_I\alpha_H}{2k_\perp L}) + \sigma_\varphi\eta_{1m} = 0. \tag{41}$$

Solving this equation gives

$$x_0 = \frac{1}{2I}\{\sigma_\varphi+\eta_{1m}-i\alpha_P+\sigma_\varphi\frac{\alpha_I\alpha_H}{2k_\perp L} \pm[(\sigma_\varphi+\eta_{1m}-i\alpha_P+\sigma_\varphi\frac{\alpha_I\alpha_H}{2k_\perp L})^2-4\sigma_\varphi\eta_{1m}I]^{1/2}\}$$
$$\simeq \frac{1}{2I}[\sigma_\varphi+\eta_{1m}-i\alpha_P+\sigma_\varphi\frac{\alpha_I\alpha_H}{2k_\perp L}\pm(a+ib)^{1/2}], \tag{42}$$

where

$$a = (\sigma_\varphi-\eta_{1m})^2-\alpha_P^2-\frac{2\eta_{1m}^2\alpha_H(\alpha_H-\alpha_I)}{k_\perp L}, \tag{43}$$

$$b = -2\alpha_P(\sigma_\varphi+\eta_{1m}), \tag{44}$$

and

$$I = 1+\frac{\alpha_H^2}{2k_\perp L}\simeq 1. \tag{45}$$

In expressions (43) and (44) the small terms of the order of $1/(k_\perp L)^2$ are neglected.

Using a formula for the square root of a complex number [e.g., *Abramowitz and Stegun*, 1964]

$$(a+bi)^{1/2} = \pm 2^{-1/2}\cdot$$
$$\left\{\left[(a^2+b^2)^{1/2}+a\right]^{1/2}+i\ \mathrm{sgn}\ b\left[(a^2+b^2)^{1/2}-a\right]^{1/2}\right\}, \tag{46}$$

we obtain

$$\mathrm{Re}x_0 = (2I)^{-1}\cdot\left\{\sigma_\varphi+\eta_{1m}+\sigma_\varphi\frac{\alpha_I\alpha_H}{2k_\perp L}\eta_{1m}\pm\left[\frac{(a^2+b^2)^{1/2}+a}{2}\right]^{1/2}\right\}, \tag{47}$$

and

$$\gamma = (2I)^{-1}\left\{-\alpha_P\mp\left[\frac{(a^2+b^2)^{1/2}-a}{2}\right]^{1/2}\right\}. \tag{48}$$

Expressions (47) and (48) are still difficult to analyze because they depend on both $k_\perp$ and φ. We can further simplify the problem by considering only those wave angles at which the maximum growth occurs. Maximizing the growth rate (48) over σ_φ in the leading order gives

$$\sigma_\varphi = \eta_{1m}+\alpha_P\simeq\eta_{1m}. \tag{49}$$

Eliminating σ_φ from (47) and (48) with the help of (49), we get

$$\Delta\eta_{1m}\simeq\pm 2^{-1/2}\{[(\frac{\eta_{1m}^2\alpha_H(\alpha_H-\alpha_I)}{2k_\perp L})^2+\alpha_P^2\eta_{1m}^2]^{1/2} - \frac{\eta_{1m}^2\alpha_H(\alpha_H-\alpha_I)}{2k_\perp L}\}^{1/2}, \tag{50}$$

and

$$\gamma\simeq-\frac{\alpha_P}{2}\mp 2^{-1/2}\{[(\frac{\eta_{1m}^2\alpha_H(\alpha_H-\alpha_I)}{2k_\perp L})^2+\alpha_P^2\eta_{1m}^2]^{1/2} + \frac{\eta_{1m}^2\alpha_H(\alpha_H-\alpha_I)}{2k_\perp L}\}^{1/2}, \tag{51}$$

where $\Delta\eta_{1m}$ is the frequency shift and the bottom sign gives an instability.

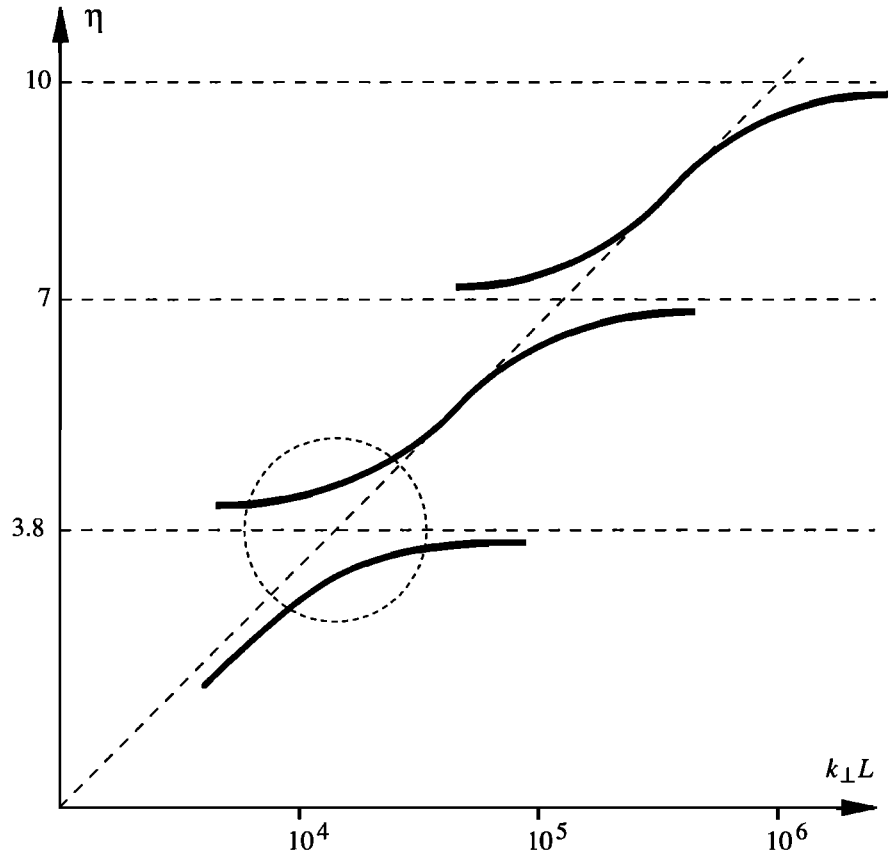

Figure 2. Modification of the IAR eigenmodes due to the Hall dispersion.

Using the explicit expression for σ_φ (36) and omitting the small term, we rewrite condition (49) in the form

$$\cos(\varphi - \arctan\frac{\alpha_P}{\alpha_H}) = -\frac{v_{1m}^{cr}}{v_0}, \tag{52}$$

with

$$v_{1m}^{cr} = \frac{\alpha_I c_{A0}\eta_{1m}}{k_\perp L \alpha_C}. \tag{53}$$

According to (52) the angle φ corresponding to the maximum growth exists if $v_0 \geq v_0^{cr}$, which defines the instability threshold. When $v_0 = v_0^{cr}$, we have $\varphi = \varphi_{\max}$ with

$$\varphi_{\max} \simeq \pm\pi + \arctan\frac{\alpha_P}{\alpha_H}. \tag{54}$$

Substituting $\varphi = \varphi_{\max} + \Delta\varphi$ into equation (52) and using the expansion $\cos\Delta\varphi \simeq 1 - (\Delta\varphi)^2/2$, we obtain that such an angle exists in the cone

$$\varphi_{\max} - [2(1 - \frac{v_{1m}^{cr}}{v_0})]^{1/2} < \varphi < \varphi_{\max} + [2(1 - \frac{v_{1m}^{cr}}{v_0})]^{1/2}, \tag{55}$$

centered around $\varphi_{\max}$. This situation is similar to the Čerenkov radiation in collisionless plasma. For the marginal instability ($v_0 \simeq v_0^{cr}$) the growing waves propagate at an angle defined by equation (54). The growing mode has negative frequency shift (red shift).

When $\alpha_P \gg \eta_{1m}\alpha_H(\alpha_H - \alpha_I)/k_\perp L$, the Pedersen term is dominant and equations (50) and (51) reduce to the result of *Lysak* [1991],

$$\Delta\eta_{1m} = \pm\left(\frac{\alpha_P\eta_{1m}}{2}\right)^{1/2}, \tag{56}$$

and

$$\gamma = -\frac{\alpha_P}{2} \mp \left(\frac{\alpha_P\eta_{1m}}{2}\right)^{1/2}. \tag{57}$$

In the opposite case when $\eta_{1m}\alpha_H(\alpha_H - \alpha_I)/k_\perp L \gg \alpha_P$, the Hall term is dominant. Thus (50) and (51) reduce to

$$\Delta\eta_{1m} = \pm\frac{\alpha_P}{\alpha_H}[k_\perp L/2(1 - \alpha_I/\alpha_H)]^{1/2}, \tag{58}$$

and

$$\gamma = \mp\frac{\eta_{1m}\alpha_H(1 - \alpha_I/\alpha_H)^{1/2}}{(2k_\perp L)^{1/2}} - \frac{\alpha_P}{2}. \tag{59}$$

Comparing (51) and (57), we note that in general the inclusion of the Hall dispersion in the IAR model enhances the feedback instability growth rate. This is connected with the decrease of the phase velocity of IAR eigenmodes caused by the Hall dispersion frequency shift. In this case the wave moves more slowly and stays longer in resonance with the convective flow.

In general, the Hall conductivity in the ionosphere scales with the Pedersen conductivity. For example, for sunlight-produced conductivity, the ratio $\alpha_H/\alpha_P \sim 2$, while for precipitation-produced conductivity, their ratio scales as $\alpha_H/\alpha_P \sim E^{5/8}$ [e.g., *Spiro et al.*, 1982], where E is energy of precipitating electrons in keV. This ratio is 6.5 for energy of 20 keV and 8.4 for energy of 30 keV. Thus the conductivity α_C in equation (36) is related to the Pedersen conductivity α_P by the relation $\alpha_C = \alpha_P(1 + E^{5/4})^{1/2}$. Using this connection, we can estimate from (51) the relative contribution of the Hall and Pedersen terms in the feedback instability growth rate given by

$$\frac{\eta_{1m}\alpha_H(\alpha_H - \alpha_I)}{k_\perp L \alpha_P} \simeq \frac{\eta_{1m}\alpha_P E^{5/4}}{k_\perp L}. \tag{60}$$

From (60) we obtain that the relative role of Hall dispersion in the feedback instability increases with both the growth of the wavelength and the energy of precipitating electrons. This contribution becomes stronger for the highest harmonics of IAR eigenmodes. However, the actual role of the Hall dispersion corrections in the feedback instability growth rate is not very high. This is supported by the following estimations. The parameter $k_\perp L = 2\pi L/\lambda_\perp$ ($\lambda_\perp$ is the perpendicular wavelength) is 60 for a wavelength of 100 km, and 6000 for 1 km. A reasonable value for the normalized nighttime Pedersen conductivity α_P is 0.1 [e.g., *Spiro et al.*, 1982]. Substituting these values into (60), it is found that the Hall correction term only becomes significant in the long-wavelength limit. It should be noted that in this case the effects of finite $k_\perp d$ which we omitted in the derivation of boundary condition (16) should also be accounted for. The importance of the Hall terms in the study of shear Alfvén waves in the auroral region was also emphasized recently by *Yoshikawa and Itonaga* [1996]. However, for most typical auroral structures with wavelengths of the order of $1 - 10$ km the Hall dispersion effects are negligible, and the previous analysis of *Lysak* [1991] serves as a reasonable approach to the problem at hand.

6. Feedback Instability in the Highly Conductive Ionosphere

When the ionospheric conductivity is high, the IAR eigenfrequencies are localized near the roots of the zero order Bessel function $J_0(\eta_{0m}) = 0$. Expansion of (38) in the vicinity of $x_0 \simeq \eta_{0m}$ in the leading order gives

$$\frac{x_0(x_0 - \eta_{0m})}{(x_0 - \sigma_\varphi)} = (i\alpha_P + \frac{\eta_{0m}\alpha_H^2}{2k_\perp L})^{-1}. \tag{61}$$

Here, as in the previous section, terms containing ε and ν, as well as the corrections of the order of $1/(k_\perp L)^2$, have been neglected.

$$x_0^2 - x_0(\eta_{0m} - i\frac{1}{\alpha_P} + i\frac{\eta_{0m}^2\alpha_H^2}{2\alpha_P k_\perp L}) - i\frac{\sigma_\varphi}{\alpha_P} + i\frac{\eta_{0m}^3\alpha_H^2}{2\alpha_P k_\perp L} = 0. \tag{62}$$

Solution of this equation can be obtained by a method presented in the previous section. However, the result can be obtained even easier if we simply analyze equation (62). First, we note that contrary to the previous section, the feedback instability growth rate increases with the increase of σ_φ without approaching any maximum value. Since we neglected the nonlinear terms, our theory is valid only in the vicinity of the instability threshold when the imaginary part of x_0 vanishes. From equation (62) follows that the condition $\mathrm{Im}x_0 = \gamma = 0$ corresponds to two solutions $\sigma_\varphi = \eta_{0m}^3\alpha_H^2/2\alpha_P k_\perp L$ and $\sigma_\varphi = \eta_{0m}$. Substituting these values into equation (62) we obtain $x_0 = 0$ and $x_0 = \eta_{0m}$. The first root is unphysical and corresponds to zero frequency mode. The other solution is related to the IAR eigenmode. Thus we have to consider only the second case. Near the instability threshold we may introduce $\Delta\sigma_\varphi = \sigma_\varphi - \eta_{0m}$ and $x_0 = \eta_{0m} + \Delta\eta_{0m} + i\gamma$ with $\Delta\eta_{0m} \ll \eta_{0m}$ and $\gamma \ll \eta_{0m}$. Substituting these values into equation (62) and neglecting the terms of the order $1/(k_\perp L)^2$, we immediately obtain the expressions for the frequency shift and instability growth rate

$$\Delta\eta_{0m} = \frac{\sigma_\varphi - \eta_{0m}}{\alpha_P^2\eta_{0m}^2}, \tag{63}$$

and

$$\gamma = \frac{\sigma_\varphi - \eta_{0m}}{\alpha_P\eta_{0m}}. \tag{64}$$

Equation (64) coincides with the corresponding expression (9) of the paper by *Trakhtengertz and Feldstein* [1991] (except for the numerical factor 3), which was obtained in the absence of the Hall dispersion. Thus in accordance with our preliminary considerations made in section 3, Hall corrections (at least of the first order) are not important in the high-conductivity limit. The maximum value of σ_φ appears when $\cos[\varphi - \arctan(\alpha_P/\alpha_H)] = -1$, that is, at $\varphi = \varphi_{\max} \simeq \pm\pi + \arctan E^{-5/8}$, similar to the previous section. This angle depends only on the energy of precipitating electrons.

Substituting $\varphi = \varphi_{\max}$ into the equations (63) and (64), we finally get

$$\Delta\eta_{0m} = \frac{1}{\alpha_P^2\eta_{0m}}(\frac{v_0}{v_{0m}^{cr}} - 1), \tag{65}$$

and

$$\gamma = \frac{1}{\alpha_P}(\frac{v_0}{v_{0m}^{cr}} - 1), \tag{66}$$

where $v_{0m}^{cr} = \alpha_I\alpha_C^{-1}c_{A0}\eta_{0m}/k_\perp L$.

Instability occurs if

$$v_0 \geq v_{0m}^{cr} = \frac{c_{A0}\alpha_I\eta_{0m}}{\alpha_P k_\perp L(1 + E^{5/4})^{1/2}}. \tag{67}$$

According to (65) the growing mode has a positive frequency shift (blue shift). At high conductivity the instability moves to a larger value of σ_φ. For a given drift velocity v_0, this just implies that the wavelength

becomes shorter. Only the product of $k_\perp$ and v_0 is specified by the instability conditions. Thus a modest drift velocity can give rise to the instability for a short enough wavelength. With the increase of α_P the growth rate vanishes as $\gamma \propto \alpha_P^{-1}$ [cf. *Lysak*, 1991; *Trakhtengertz and Feldstein*, 1991].

7. Discussion and Conclusions

The analysis presented in this paper shows that the IAR feedback instability may exist at both high and low ionospheric conductivities as was predicted by *Lysak* [1991] and *Trakhtengertz and Feldstein* [1991]. Coupling of the shear Alfvén waves to the compressional mode, considered in our paper, leads to a weak dispersion of IAR eigenmodes as shown in Figure 2. In the low-conductivity limit $\alpha_P \ll 1$ the inclusion of the Hall conductivity terms leads to the increase in the feedback instability growth rate, which is caused by the reduction of the phase velocity of the IAR eigenmodes. However, for real ionospheric parameters this modification is not very strong. It should be noted that the ionospheric conductivity is low mainly during the nighttime conditions. In this case the ionospheric dissipation is small, and the electric field of magnetospheric convection can easily penetrate the conductive slab. Thus the convection flow moves relatively freely through the ionosphere, losing its energy due to Čerenkov radiation in the IAR. This situation is similar to one in the toroidal magnetospheric waveguide, in which the ordinary mechanisms of energy dissipation (such as wave absorption at the ends of the geomagnetic field line tubes) are not present [*Pokhotelov et al.*, 1997, 1998]. When ionospheric conductivity is high (daytime), the feedback instability may also arise, but the growing oscillations shift to shorter wavelengths.

Recently, *Newell et al.* [1996] presented data from the DMSP satellite showing that the most intense auroral arcs (discrete aurora), which are usually attributed to the small-scale Alfvénic structures, appear preferentially in the weakly conducting ionosphere when strong electron precipitation is observed. The analysis presented here shows that the feedback instability growth rate scales with the ionospheric conductivity as $\alpha_P^{1/2}$ during the nighttime (low conductivity) and as α_P^{-1} during daytime (high conductivity). Thus the preferable conditions for strongest deceleration of the convective flow and subsequent excitation of IAR eigenmodes are probably realized during periods of low ionospheric conductivity, in accordance with the data of *Newell et al.* [1996]. These authors also came to the same conclusions and considered that the model developed by *Lysak* [1991] is the most probable candidate to explain the appearance of discrete auroral arcs among other 22 theories of auroral arcs discussed by *Borovsky* [1993].

For more comprehensive comparison with the observational data our analysis should be supplemented by the numerical study of dispersion relation (38). *Lysak* [1991] has performed numerical investigation using a similar dispersion relation that does not include the Hall dispersion corrections. This analysis revealed the appearance of the growth rate maximum at $\alpha_P \simeq 1$, that is, when the IAR is optimally matched with the magnetospheric load. Results from the numerical analysis of the IAR feedback instability using equation (38) with arbitrary values of ionospheric conductivity will be presented in a separate paper.

The results of our study might be useful for a better understanding of the fundamental IAR properties, as well as for the interpretation of recent satellite observations by Freja and Fast satellites [e.g., *Stasiewicz and Potemra*, 1998; *Ergun et al.*, 1998].

Acknowledgments. We are grateful to Robert Lysak and an other referee for stimulating comments and fruitful discussions. The authors acknowledge financial support from the Commission of the European Union (grant INTAS-96-2064), from the Russian Foundation for Basic Research (grant 97-05-64606), and from NASA (grants NAG5-2252 and NAG5-4529). Two of us (O.P. and A.S.) appreciate financial support from ISSI through the project "Small Alfvénic Structures in the Magnetosphere". We thank Bengt Hultqvist for warm hospitality at ISSI, where this paper was discussed with the members of the project. One of us (O.P.) wishes to thank the French Ministère de la Recherche et de la Technologie for hospitality at LPCE, where this work was completed.

Michel Blanc thanks Robert Lysak and another referee for their assistance in evaluating this paper.

References

Abramowitz, M., and I. A. Stegun, *Handbook of Mathematical Functions*, U.S. Nat. Inst. of Standards and Technol., Gaithersburg, Md., 1964.

Atkinson, G., Auroral arcs: Result of the interaction of a dynamic magnetosphere with the ionosphere, *J. Geophys. Res., 75*, 4746, 1970.

Belyaev, P. P., S. V. Polyakov, V. O. Rapoport, and V. Y. Trakhtengertz, Discovery of the resonance spectrum structure of atmospheric electromagnetic noise background in the range of short-period geomagnetic pulsations, *Dokl. Akad. Nauk SSSR, 297*, 840, 1987.

Belyaev, P. P., S. V. Polyakov, V. O. Rapoport, and V. Y. Trakhtengertz, The ionospheric Alfvén resonator, *J. Atmos. Terr. Phys., 52*, 781, 1990.

Belyaev, P. P., T. Bösinger, S. V. Isaev, and J. Kangas, First evidence at high latitudes for the ionospheric Alfvén resonator, *J. Geophys. Res., 104*, 4305, 1999.

Borovsky, J. E., Auroral arc thickness as predicted by various theories, *J. Geophys. Res., 98*, 6101, 1993.

Brown, R. R., Electron precipitation in the auroral zone, *Space Sci. Rev., 5*, 311, 1966.

Ergun, R. E., et al., Fast satellite observations of electric field structures in auroral zone, *Geophys. Res. Lett., 25*, 2025, 1998.

Gradshteyn, I. S., and I. M. Ryzhik, *Tables of Integrals, Series and Products*, Academic Press, New York, 1980.

Lysak, R. L., Feedback instability of the ionospheric resonant cavity, *J. Geophys. Res., 96*, 1553, 1991.

Newell, P.T., C.-I. Meng, and K. M. Lyons, Suppression of discrete aurora by sunlight, *Nature, 381*, 766, 1996.

Pokhotelov, O. A., D. O. Pokhotelov, F. Z. Feygin, M. Parrot, K. Hayashi, J. Kangas, and K. Mursula, Oxygen cyclotron harmonic waves in the deep plasmasphere during magnetic storms, *J. Geophys. Res., 102*, 77, 1997.

Pokhotelov, O. A., D. O. Pokhotelov, F. Z. Feygin, V. A. Gladychev, M. Parrot, J. Kangas, K. Mursula, P. K. Shukla, and L. Stenflo, Excitation of helium cyclotron harmonic waves during quiet magnetic conditions, *J. Geophys. Res., 103,* 26,5857, 1998.

Polyakov, S. V., On the properties of the ionospheric Alfvén resonator, in: *KAPG Symposium on Solar-Terrestrial Physics,* vol. 3, pp. 72-73, Nauka, Moscow, 1976.

Polyakov, S. V., and V. O. Rapoport, The ionospheric Alfvén resonator, *Geomagn. Aeron., 21,* 816, 1981.

Rees, M. H., Auroral ionization and excitation by incident energetic electrons, *Planet. Space Sci., 11,* 1209, 1963.

Rothwell, P. L., M. B. Silevitch, and L. P. Block, A model for propagation of the westward traveling surge, *J. Geophys. Res., 89,* 8941, 1984.

Sato, T., A theory of quiet auroral arcs, *J. Geophys. Res., 83,* 1042, 1978.

Sato, T., and T. E. Holzer, Quiet auroral arcs and electrodynamic coupling between the ionosphere and the magnetosphere, *J. Geophys. Res., 78,* 7314, 1973.

Spiro, R. W., P. H. Reiff, and L. J. Maher, Precipitating electron energy flux and auroral zone conductances: An empirical model, *J. Geophys. Res.,* 87, 8215, 1982.

Stasiewicz, K., and T. Potemra, Multiscale current structures observed by Freja, *J. Geophys. Res., 103,* 4315, 1998.

Trakhtengertz, V. Y., and A. Y. Feldstein, Turbulent Alfvén boundary layer in the polar ionosphere, 1, Excitation conditions and energetics, *J. Geophys. Res., 96,* 19,363, 1991.

Watson, G. N., *Theory of Bessel Functions,* p. 227, Cambridge Univ. Press, New York, 1948.

Yoshikawa A., and M. Itonaga, Reflection of shear Alfvén waves at the ionosphere and the divergent Hall current, *Geophys. Res. Lett., 23,* 101, 1996.

V. Khruschev, O.A. Pokhotelov, Institute of Physics of the Earth, 123810 Moscow, B. Gruzinskaya 10, Russia. (e-mail: pokh@uipe-ras.scgis.ru)

M. Parrot,Laboratoire de Physique et Chimie de l'Environnement, Centre National de la Rechercher Scientifique, 45071 Orléans Cedex 02, France. (e-mail: mparrot@cnrs-orleans.fr)

D. Pokhotelov, A. Streltsov, Thayer School of Engineering, Dartmouth College, Hanover, NH 03755.

(Received April 19, 1999; revised October 11, 1999; accepted October 18, 1999.)